UCRL--95397

DE87 000601

Single Particle Effects in Precompound Decay Reactions

M. Blann
T. Komoto
G. Reffo
F. Fabbri
S. M. Grimes

This paper was prepared for submittal to the Proceedings of the IAEA Conference in Bologna, Italy

September 1986

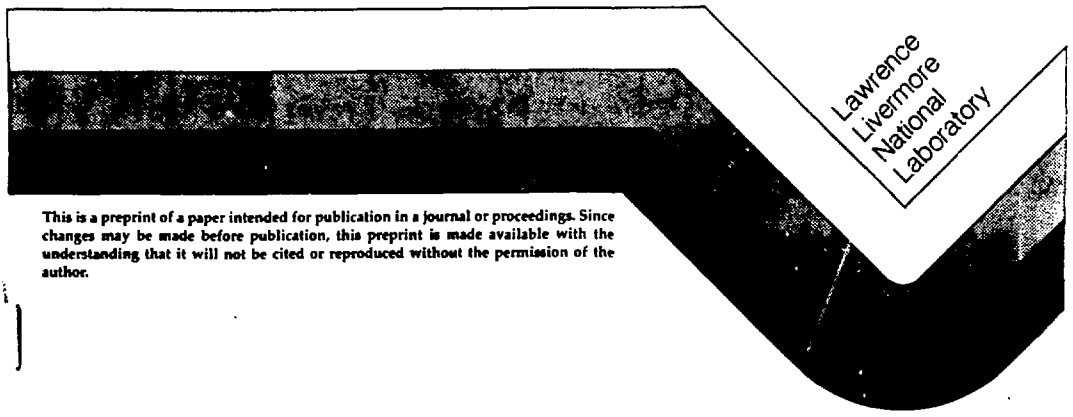

Single Particle Effects in Precompound Decay Reactions

M. Blann and T. Komoto
Lawrence Livermore National Laboratory
Livermore, California, U.S.A.

G. Reffo and F. Fabbri
ENEA, Bologna, Italy

and

S. M. Grimes
Physics Department
Ohio University
Athens, Ohio, U.S.A.

1. Introduction

Precompound decay models generally rely on use of a partial state density (PSD) formula which is generated using an assumed equidistantly spaced set of single particle levels. We expect this to be a reasonable assumption for mid-shell nuclei; however it has been demonstrated [1,2] that quite large errors may be introduced by making the equidistant spacing assumption for nuclei which have neutron or proton numbers near or at major shell closures. In this work we wish to review the simple qualitative considerations of those deviations expected for near closed shell nuclei, compare these expectations with experimental results, and then begin steps to implement use of partial state densities calculated with more realistic sets of single particle levels in precompound decay calculations. We will do this for the case of Zr targets.

2. Qualitative Considerations

A (p,n) precompound reaction should result primarily from neutron emission from a three quasiparticle configuration characterized by a pnn^{-1} description, leaving a residual nucleus of pn^{-1} character. Consider the shell model representation of the target nuclei $^{90,91,92,94}Zr$ in Figure 1, where the neutron levels are represented[3]. Consider a (p,n) reaction on these targets. In the case of ^{90}Zr, any one of ten ($g_{9/2}$) neutrons may be ejected to give a ground state product. For slightly more energy, 8 neutrons ($p_{1/2}$, $f_{5/2}$) may be ejected. We therefore expect the precompound $^{90}Zr(p,n)$ spectra to start with a large ground state cross section, and continue to higher residual excitations with high cross sections.

For the $^{91}Zr(p,n)$ reaction, we can only populate the ground state if the single $d_{5/2}$ neutron is ejected. If this is not the case, there is a 4 MeV gap in order to eject one of the ten $g_{9/2}$ neutrons. We could therefore expect a small ground state peak, a large gap, followed by a spectrum which otherwise resembled that of $^{90}Zr(p,n)$.

For $^{92,94}Zr(p,n)$ we would expect larger ground state transitions than for $^{91}Zr(p,n)$. Because nuclear deformation should increase with increasing neutron number, we might expect the 4 MeV gap to decrease for the heavier target isotopes.

In Figure 2 we show experimental (p,n) spectra from these four target isotopes compared with geometry dependent hybrid model calculations[4]. The qualitative expectations discussed above are observed, and it is seen that the GDH model precompound calculations with equidistant level spacings (ESM) are unable to reproduce the nuclear structure effects noted. This is not the case for mid-shell nuclei, as is shown in Figure 3. We therefore wish to replace the ESM densities with values calculated using shell model single particle orbitals. The method used to do this was by use of recursion relationships, as originally programmed by Williams, and later modified by Albrecht and by Grimes.[1,2,5,6] A brief description of the method used is given below, much quoted directly from (3).

3. Calculation of Few Quasiparticle Densities

The few exciton state densities $\omega(Q,N)$ for N similar fermions above the Fermi energy with a total excitation energy Q are calculated from a set of single particle energies $\epsilon = E_i - E_F$ measured with respect to the target Fermi eneergy[2] E_F using the recursion relation [1]

$$\omega_i(Q,N)=\omega_{i-1}(Q,N)+\omega_{i-1}(Q-\epsilon_i,N-1). \qquad (1)$$

The recursion index i refers to the ith single particle energy. The state density $\omega(U,N_H)$ for N_H holes that share the excitation energy U can be similarly calculated. The recursion converges rapidly. Results are then folded to give the particle-hole state density $\omega(Q,N,N_H)$:

$$\omega(Q,N,N_H) = \sum_{U=0}^{Q} \omega(U,N)\omega(Q-U,N_H). \qquad (2)$$

If both kinds of nucleons share the excitation energy E*, an equivalent calculation based on the corresponding set of single particle levels gives $\omega(Q,Z,Z_H)$. Folding of both results yields the final partial state density,

$$\omega(E^*,N,N_H,Z,Z_H) = \sum_{Q=0}^{E^*} \omega(Q,Z,Z_H)\omega(E^* - QN,N_H). \qquad (3)$$

These densities are defined by energy only; no information is maintained on the angular momentum distribution; this is one possible shortcoming of the present approach. Work by Reffo and his collaborators offers the possibility to remedy this situation.

The subroutines used presently allow a choice of any of three sets of internally generated single particle levels, or the option of reading in an arbitrary set of levels. The internally generated single particle sets are those due to Nilsson,[7] Seeger-Howard[8] and Seeger-Perisho.[9] A BCS pairing treatment is used,[10] and the nuclear deformation is an input parameter. For pairing in this work we use $\delta = 11/\sqrt{A}$, unless otherwise noted. The final state densities are averaged over a Gaussian averaging function which approximates various causes of level broadening, as well as facilitating comparisons with data which are broadened due to experimental resolution.

4. Implementation of Few Quasiparticle Densities into Code ALICE

Figure 2 shows that the contribution of the 3 quasiparticle decay dominates the high kinetic energy region of the spectra. We therefore will use 'realistic' partial state densities only for the two and three quasiparticle configurations in our hybrid model precompound decay calculation, using the equidistant spacing model for higher order terms.

Before proceeding further, let us summarize some of the difficulties in the calculation:

1. The calculation considers only the energies of the single particle levels; however, each residual interaction and coupling of the angular momenta of unpaired particles should yield different level energies rather than the degenerate results assumed in our codes.

2. The targets used, due to being closed shell or near closed shell in nature, involve single particle orbitals which may have very large ranges of angular momenta to which they may couple. The reaction kinematics may strongly select against population of some of these levels due to the kinematically allowed orbital angular momentum transfers. These restrictions are not considered (as yet) in our codes for generating few quasiparticle densities.

3. Positions calculated for excited single particle levels will be even more sensitive to details of the shape of the assumed potential well than for lower lying orbitals.

4. As particle orbitals become unbound, the shell model levels become questionable in meaning; the centrifugal barrier, and for protons the Coulomb barrier may mitigate this point for a few MeV. (For ^{90,91,92,94}Nb, the proton binding energies are 5.2, 5.8, 6.0, and 6.8 MeV, respectively.)

5. As the single particle energies increase the lifetime decreases, and the natural width due to the Heisenberg principle increases. Similarly, the spreading width will change. We might therefore expect that the constant averaging width of our calculation might better be replaced by an energy dependent function.

With these caveats in mind, our first goal is to get some improvement over results using ESM. We may then concentrate attention on improving the treatment of the partial state densities for some of the objections noted above.

For neutron induced reactions we compute the following PSD tables: nnn^{-1}, npp^{-1}, nn^{-1}, pp^{-1}, and np^{-1}. For proton induced reactions we compute ppp^{-1}, pnn^{-1}, pp^{-1}, pn^{-1}, and nn^{-1}. These results are calculated for excitation energies up to 20 MeV. Above that energy the values at 20 MeV are extrapolated using the ESM energy dependence for each exciton number. The expressions used for the decay of the three quasiparticle states are given by the following:

for n,n'

$$\frac{d\sigma}{dE} = \sigma_R\left[\frac{0.5\rho(nn^{-1},U)}{\rho(n^2n^{-1},E)} + \frac{0.75\rho(pp^{-1},U)}{\rho(pnp^{-1},E)}\right]\left[\frac{\lambda_c(E)}{\lambda_c(E)+\lambda_+(E)}\right]$$

where the second set of square brackets represents the fraction of the nucleons at energy ϵ which are emitted;

for (n,p), we use

$$\frac{d\sigma}{dE} = \sigma_R\left[\frac{0.75\rho(np^{-1},U)}{\rho(pp^{-1}n,E)}\right]\left[\frac{\lambda_c(E)}{\lambda_c(E)+\lambda_+(E)}\right]$$

for (p,n) we use

$$\frac{d\sigma}{dE} = \sigma_R\left[\frac{0.75\rho(pn^{-1},U)}{\rho(pp^{-1}n,E)}\right]\left[\frac{\lambda_c(E)}{\lambda_c(E)+\lambda_+(E)}\right]$$

and for p,p',

$$\frac{d\sigma}{dE} = \sigma_R\left[\frac{0.75\rho(nn^{-1},U)}{\rho(pp^{-1}n,E)} + \frac{0.5\rho(pp^{-1},U)}{\rho(p^2p^{-1},E)}\right]\left[\frac{\lambda_c(E)}{\lambda_c(E)+\lambda_+(E)}\right]$$

5. Results and Discussion

We present results of these calculations using single particle sets due to Seeger-Howard[8] and to Seeger-Perisho[9] in figures 3-13. Several values of the nuclear deformation parameter between 0 and 0.2 have been used to illustrate the sensitivity of results to this parameter.

We find some success in reproducing the structure effects on precompound spectra. The overall quality of fit is probably superior to the results of using ESM in Figure 2. The precompound routine in ALICE[11] has been revised to generate and use realistic partial state densities for the leading (3 exciton) term.

There is great room for improvement of these results. One goal for the future is an improved set of single particle levels. A candidate to be tried is a recent set due to P. Moller.[12] A next step would be use of PSD results with explicit dependence on angular momentum.[13] Finally, we must give consideration to using known low lying excited states to overcome the inevitable inability to predict these levels accurately via Nilsson type calculations.

Much work remains to be done in this area. We feel that these preliminary results are encouraging, and that further work is justified.

6. Acknowledgements

One of the authors (MB) wishes to express his appreciation to Dr. Enzo Menopace and the ENEA, Bologna, Italy for the hospitality and support while a major portion of this work was done. He also wishes to acknowledge the encouragement and support of R. Howerton and R. White.

This work was performed under the auspices of the U.S. Department of Energy by the Lawrence Livermore National Laboratory under contract number W-7405-ENG-48.

1044A-9/10/86

References

1. F. C. Williams, Jr., A. Mignerey, and M. Blann, Nucl. Phys. A 207, 619 (1973).

2. K. Albrecht and M. Blann, Phys. Rev. C 8, 1481 (1973).

3. W. Scobel et al., Phys. Rev. C 30, 1480 (1984).

4. M. Blann, Phys. Rev. Lett. 27, 337 (1971); 27, 700(E) (1971); 27, 1550(E) (1971); Phys. Rev. Lett. 28, 757 (1972).

5. S. M. Grimes, J. D. Anderson, J. W. McClure, B. A. Pohl, and C. Wong, Phys. Rev. C 7, 343 (1973); S. M. Grimes, J. D. Anderson, J. C. Davis, and C. Wong, ibid. 8, 1770 (1973).

6. S. M. Grimes, J. D. Anderson, and C. Wong, Phys. Rev. C 13, 2224 (1976); C. Wong, J. D. Anderson, J. C. Davis, and S. M. Grimes, ibid. 7, 1895 (1973).

7. S. G. Nilsson, K. Dan. Vidensk. Selsk. Mat.-Fys. Medd. 29, No. 16 (1955).

8. P. A. Seeger and W. M. Howard, Nucl. Phys. A238, 491 (1975).

9. P. A. Seeger and R. C. Perisho, Los Alamos National Laboratory Report No. LA3751, 1967 (unpublished).

10. J. Bardeen, L. N. Cooper, and J. R. Schrieffer, Phys. Rev. 108, 1175 (1957); L. G. Moretto, Nucl. Phys. A 182, 641 (1972) ; S. M. Grimes, in Theory and Application of Moment Methods in Many Fermion Systems, edited by B. J. Dalton, S. M. Grimes, J. P. Vary, and S. A. Williams (Plenum, New York, 1979), p. 17.

11. M. Blann, and J. Bisplinghoff, Lawrence Livermore National Laboratory Report UCID-19614, 1982 (unpublished); M. Blann, Lawrence Livermore National Laboratory Report UCID-20169, 1984 (unpublished).

12. P. Moller, private communication (1986).

13. G. Reffo et al., (1986) to be published.

Figure Captions

Figure 1: Schematic single particle level schemes for several stable Zr isotopes based on the levels due to Seeger and Howard (Ref. 8). Occupation of the $2d_{5/2}$ levels by neutrons is indicated by closed circles; level splitting due to several deformation parameters δ is shown.

Figure 2: Calculated and experimental (p,xn) spectra for proton energies of 18 and 25 MeV on targets of $^{90,91,92,94}Zr$. Solid points represent the experimental angle integrated data corrected for background and for isotopic impurities. The solid curves are results of the geometry dependent hybrid model plus evaporation model calculations. The dotted curves are the contribution of the first (n_0=3) exciton number to the total calculated neutron spectra. Arrows represent end point energies. Data are from Ref. 3.

Figure 3: Calculated and experimental results for $^{159}Tb(p,n)$. The solid curve is the $(1p)(1n)^{-1}$ two quasiparticle density for ^{159}Dy with δ=0.31 plotted as levels per 100 keV. Open points joined by line segments are the experimental angle integrated spectrum for 25 MeV proton energy. The dashed curve is the result of the geometry dependent hybrid model (GDH). The GDH and experimental results are plotted as mb/MeV vs. residual excitation. Data are from Ref. 3.

Figures 4-14: The heavy dots connected by a line represent the experimentally measured angle integrated (p,n) spectra on $^{90,91,92,94}Zr$ with 25 MeV incident protons.[3] The dotted lines represent the spectra calculated as described in the text, using single particle levels due to Seeger and Howard (S-H) or Seeger and Perisho (S-P), with deformation parameter δ as indicated.

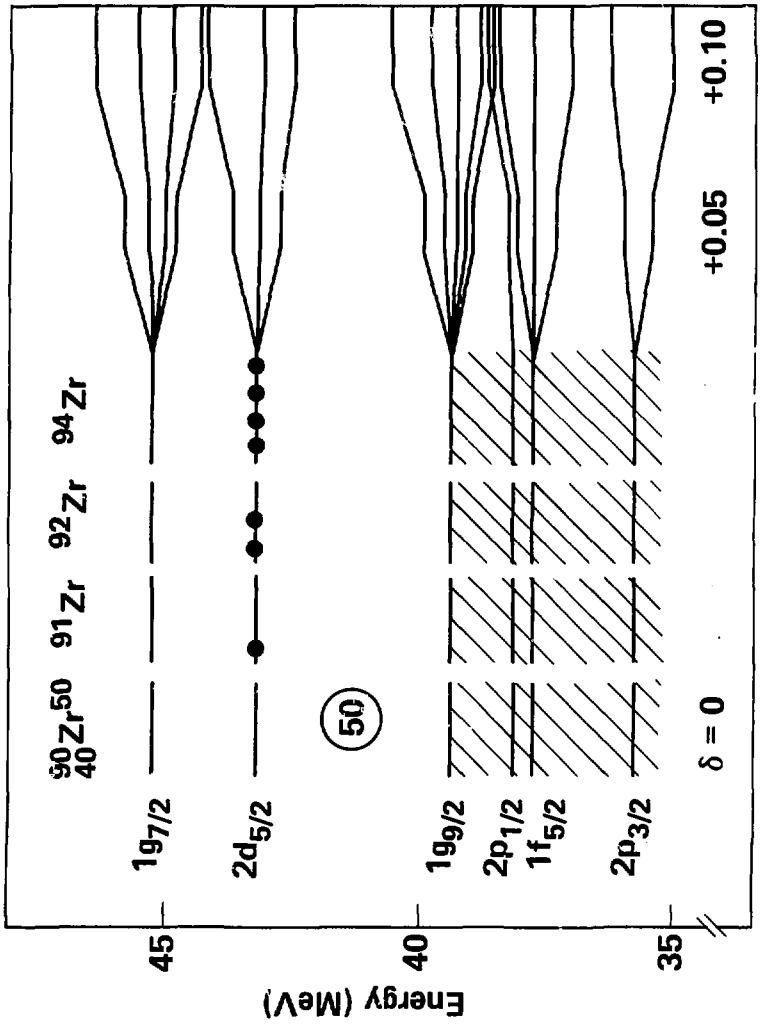
Energy (MeV)
45
40
35
$^{90}_{40}Zr_{50}$ ^{91}Zr ^{92}Zr ^{94}Zr
$1g_{7/2}$
$2d_{5/2}$
50
$1g_{9/2}$
$2p_{1/2}$
$1f_{5/2}$
$2p_{3/2}$
δ = 0
+0.05
+0.10

Figure 1

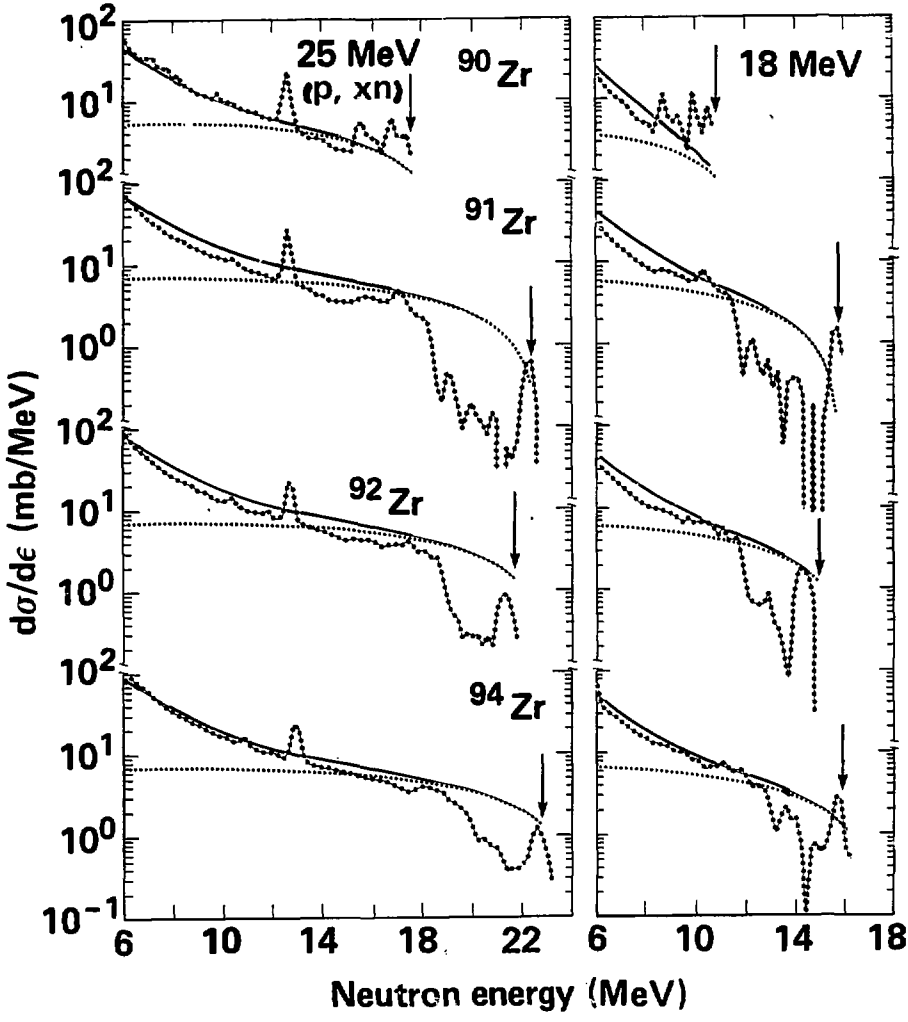
25 MeV
(p, xn)
90Zr
18 MeV
91Zr
92Zr
94Zr
dσ/dε (mb/MeV)
Neutron energy (MeV)

Figure 2

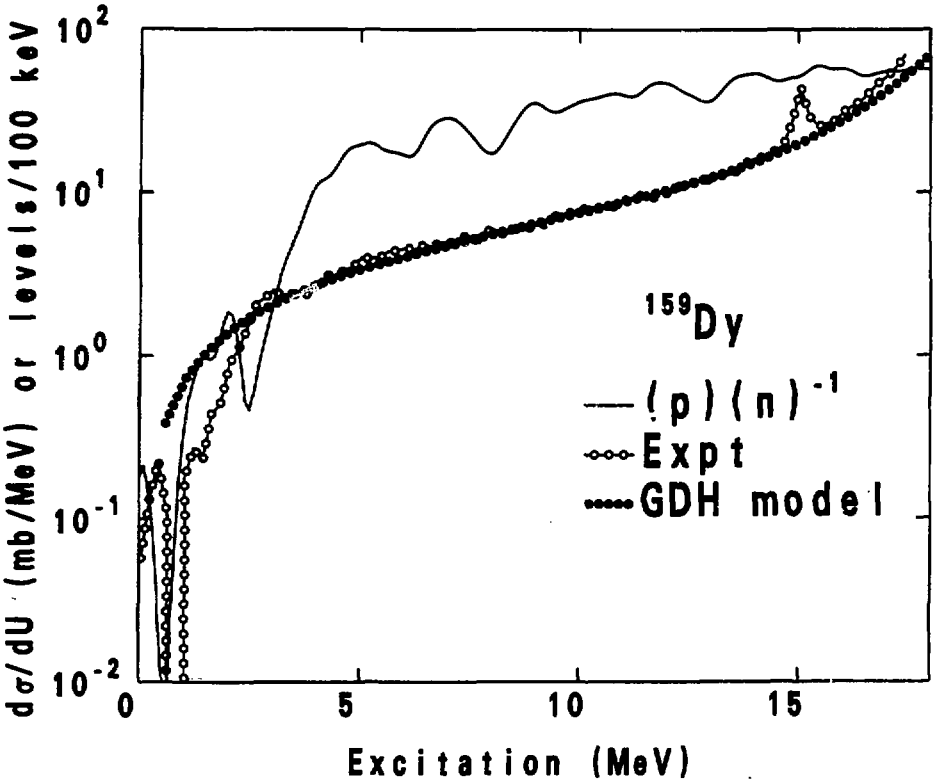
dσ/dU (mb/MeV) or levels/100 keV
10^2
10^1
10^0
10^-1
10^-2
0
5
10
15
Excitation (MeV)
159Dy
(p)(n)^-1
Expt
GDH model

Figure 3

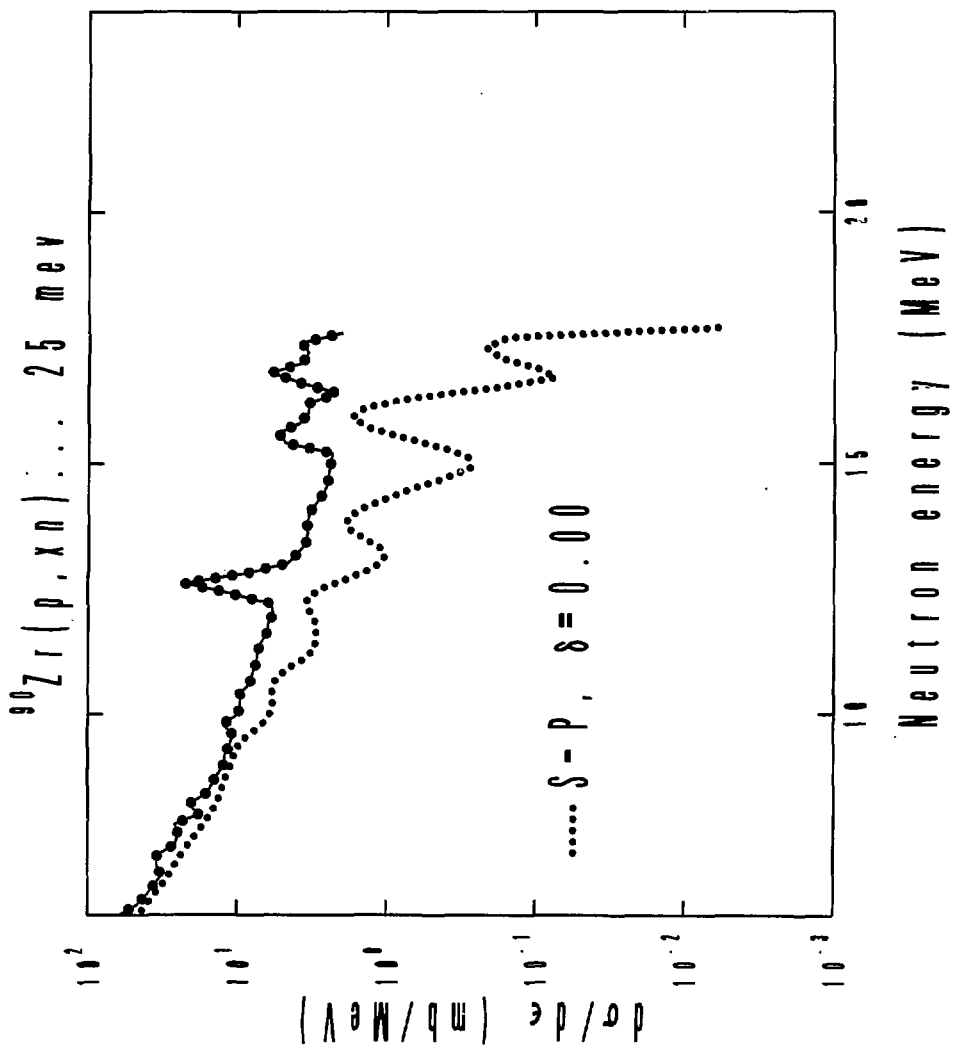
$^{90}Zr(p,xn)$.... 25 mev
.... S-P, δ=0.00
dσ/dε (mb/MeV)
Neutron energy (MeV)
10
15
20
10^{-2}
10^{-1}
10^{0}
10^{-1}
10^{-2}
10^{-3}

Figure 4

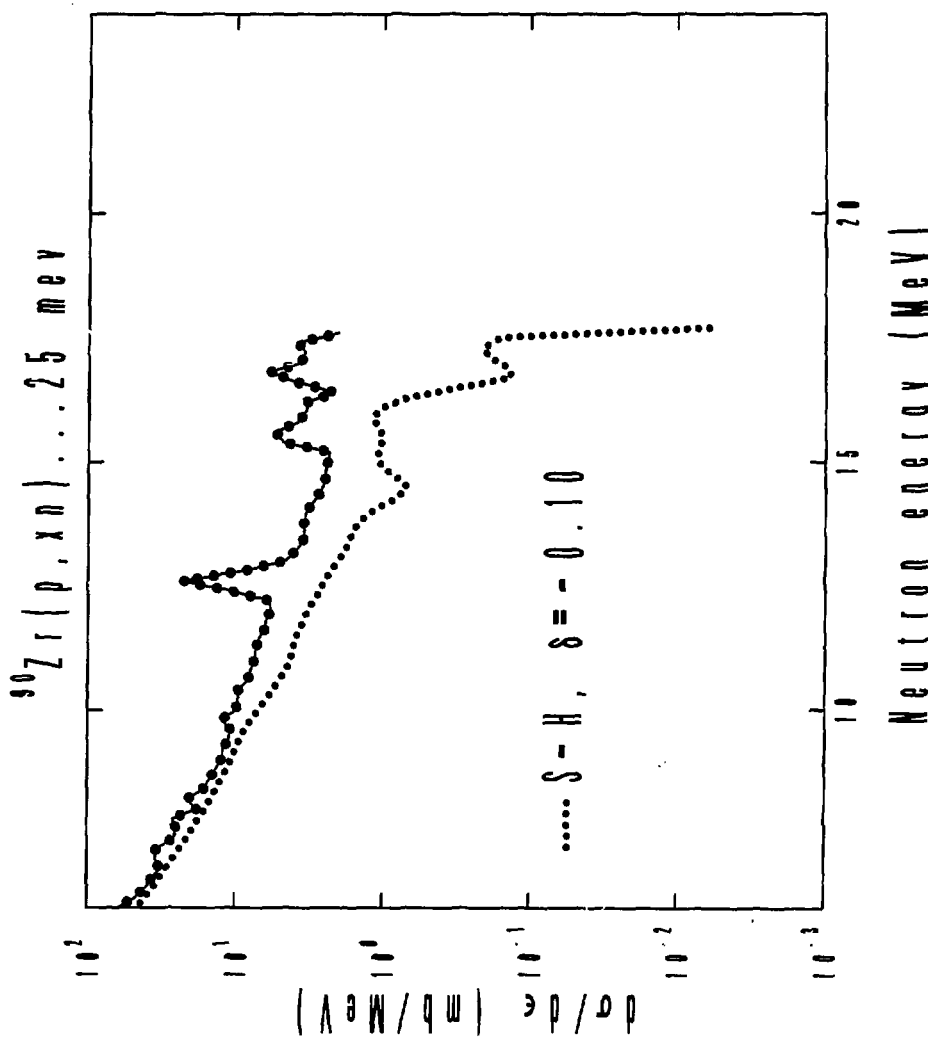
$^{90}Zr(p,xn)$....25 mev
..... S-H, δ = -0.10
$d\sigma/d\epsilon$ (mb/MeV)
Neutron energy (MeV)
10^{-2}
10^{-1}
10^{0}
10^{-1}
10^{-2}
10^{-3}
10
15
20

Figure 5

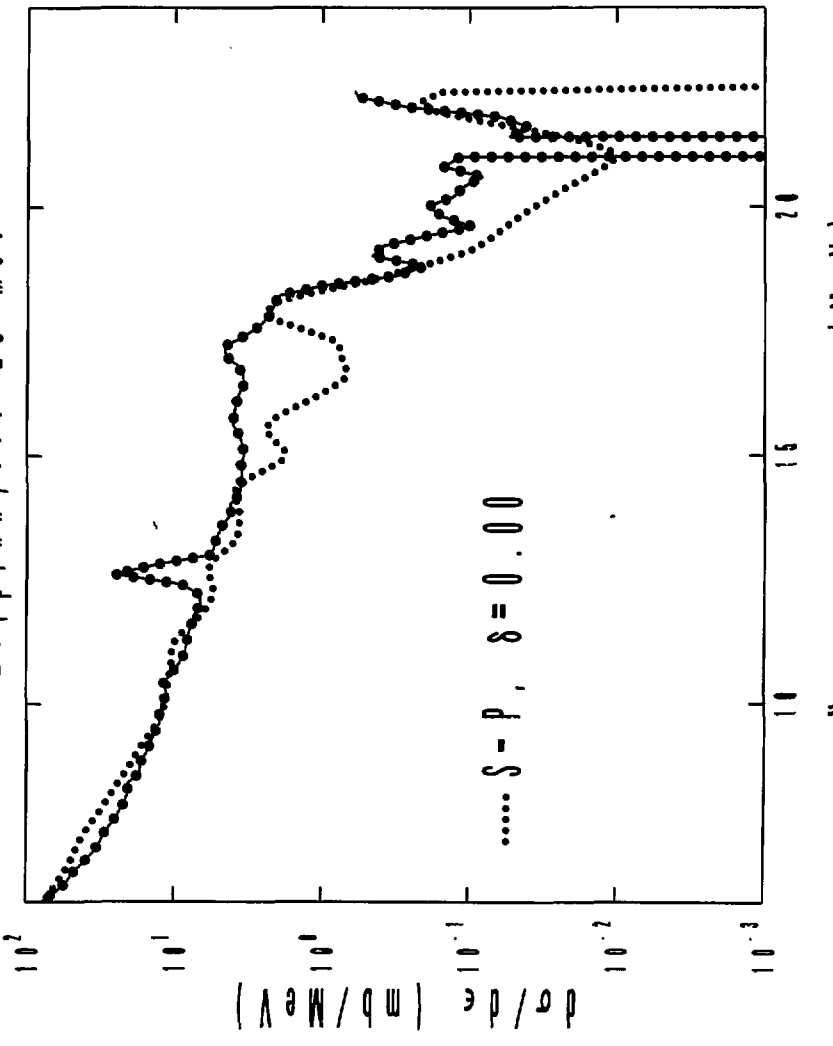
$^{91}Zr(p,xn)$.... 25 mev
..... S-P, δ=0.00
dσ/dε (mb/MeV)
Neutron energy (MeV)
10^-2
10^-1
10^0
10^-1
10^-2
10^-3
10
15
20

Figure 6

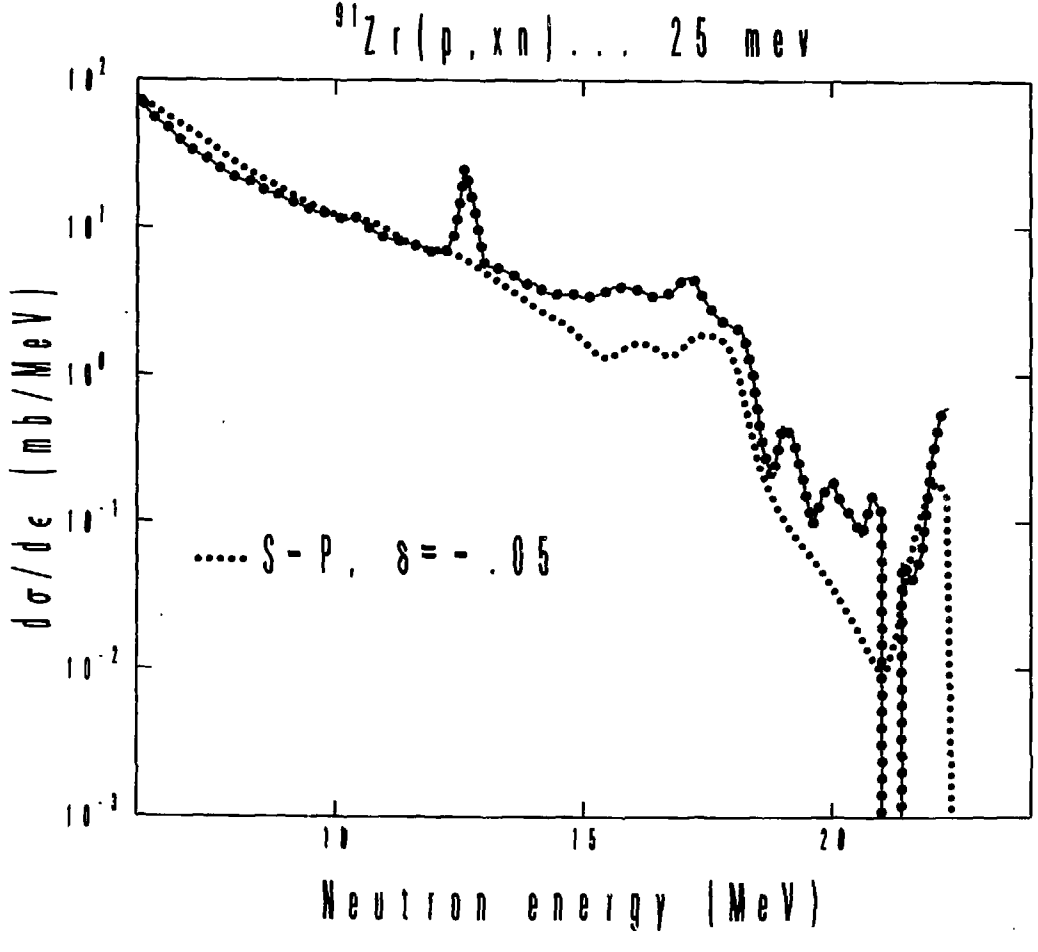
$^{91}Zr(p,xn)\ldots$ 25 mev
10^{2}
10^{1}
10^{0}
10^{-1}
10^{-2}
10^{-3}
$d\sigma/d\epsilon$ (mb/MeV)
..... S-P, δ = -.05
10
15
20
Neutron energy (MeV)

Figure 7

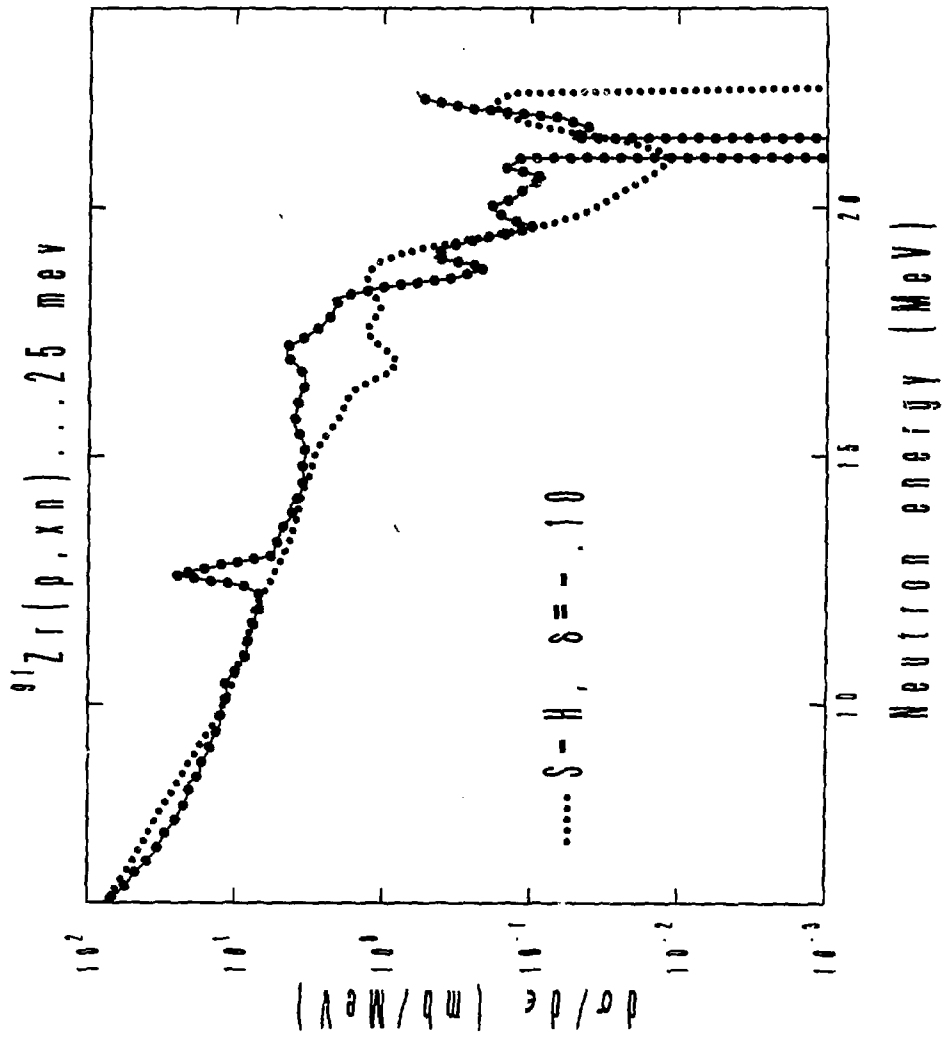
$^{91}Zr(p,xn)....25$ mev
S-H, δ = .10
$d\sigma/d\epsilon$ (mb/MeV)
Neutron energy (MeV)
10^{-2}
10^{-1}
10^{0}
10^{-1}
10^{-2}
10^{-3}
10
15
20

Figure 8

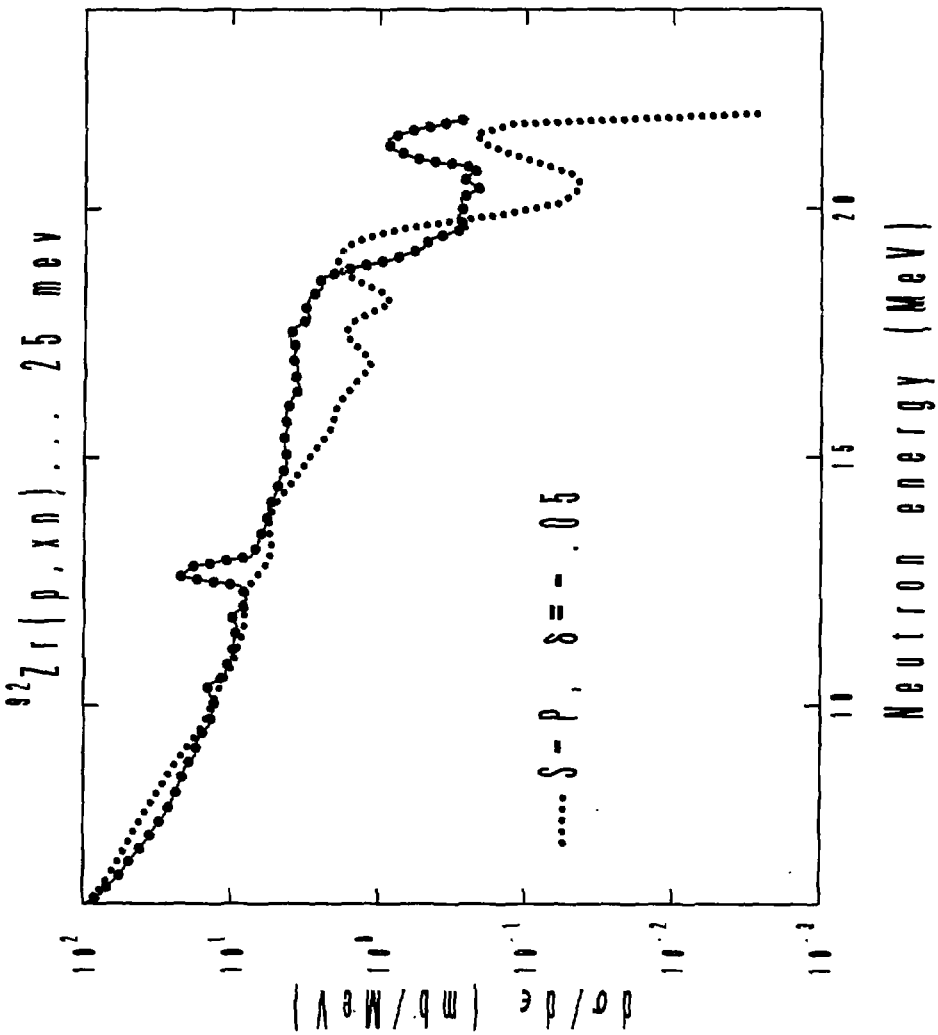
$^{92}Zr(p,xn)\ldots$ 25 mev
S-P, δ= .05
$d\sigma/d\varepsilon$ (mb/MeV)
Neutron energy (MeV)
10^{2}
10^{1}
10^{0}
10^{-1}
10^{-2}
10^{-3}
10
15
20

Figure 9

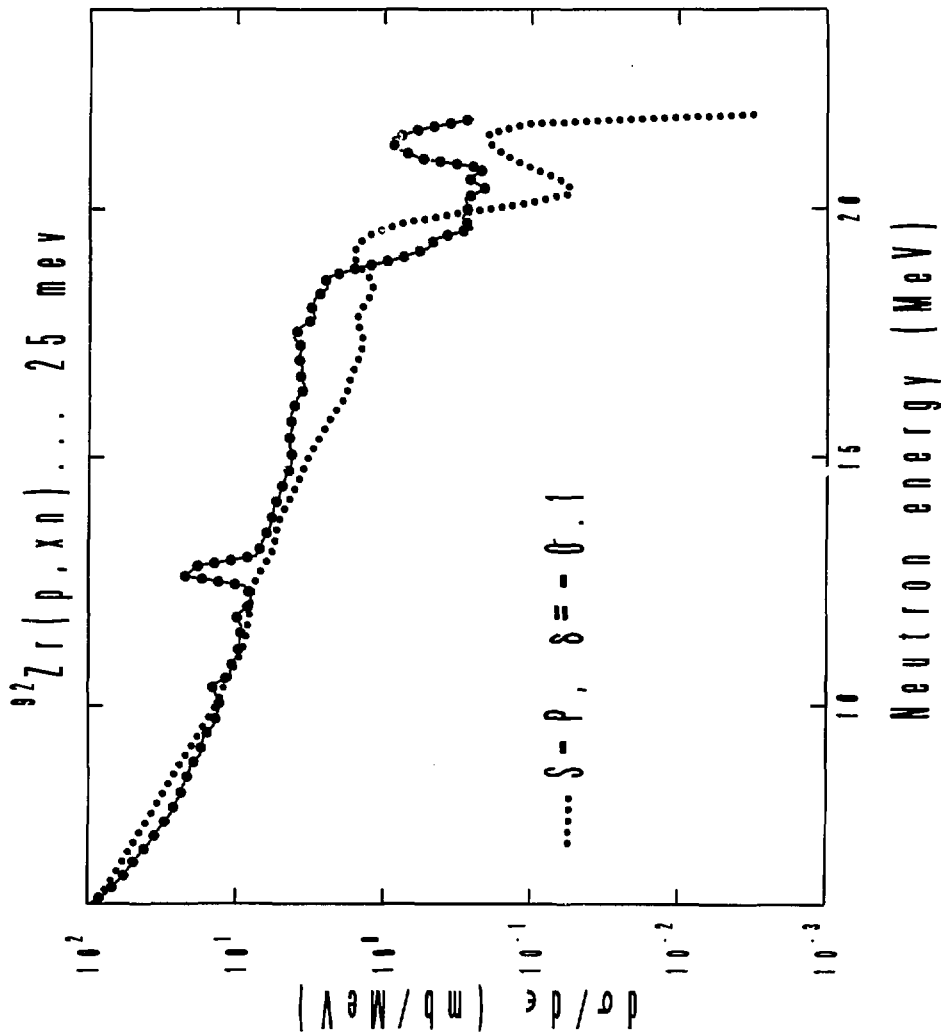
$^{92}Zr(p,xn)....25$ mev
.....S-P, δ = -0.1
$d\sigma/d\epsilon$ (mb/Mev)
Neutron energy (MeV)
10^{2}
10^{1}
10^{0}
10^{-1}
10^{-2}
10^{-3}
10
15
20

Figure 10

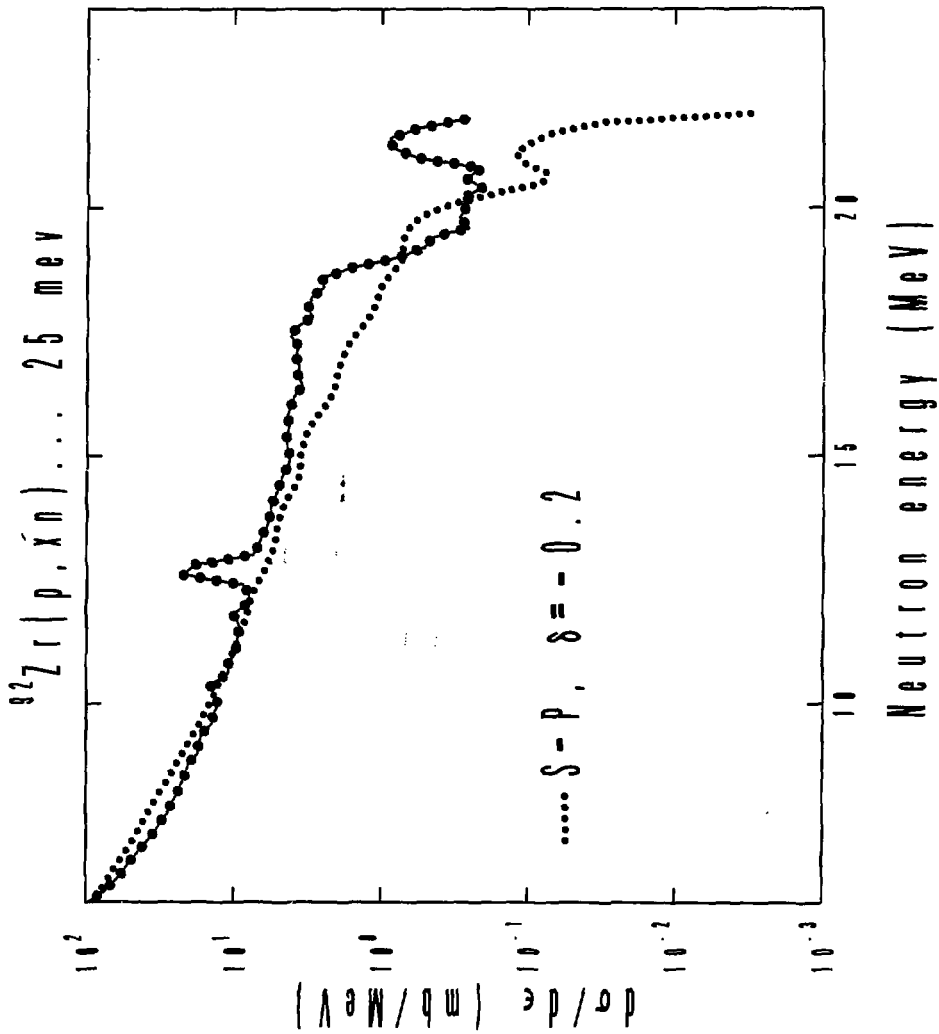
$^{92}Zr(p,xn)$.... 25 mev
..... S-P, δ = -0.2
dσ/dε (mb/MeV)
Neutron energy (MeV)
10
15
20
10^{-2}
10^{-1}
10^{0}
10^{-1}
10^{-2}
10^{-3}

Figure 11

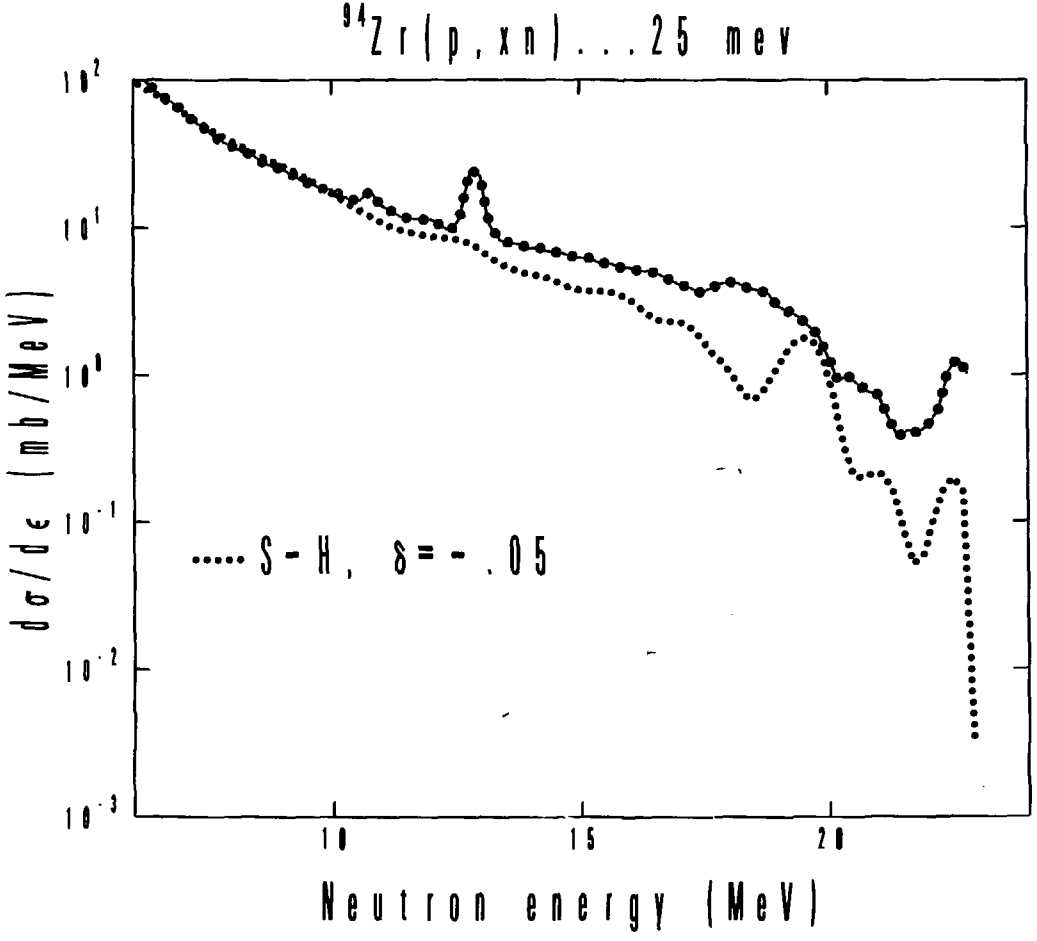
$^{94}Zr(p,xn)...25$ mev
10^{2}
10^{1}
10^{0}
10^{-1}
10^{-2}
10^{-3}
$d\sigma/d\epsilon$ (mb/MeV)
..... S-H, $\delta = -.05$
10
15
20
Neutron energy (MeV)

Figure 12

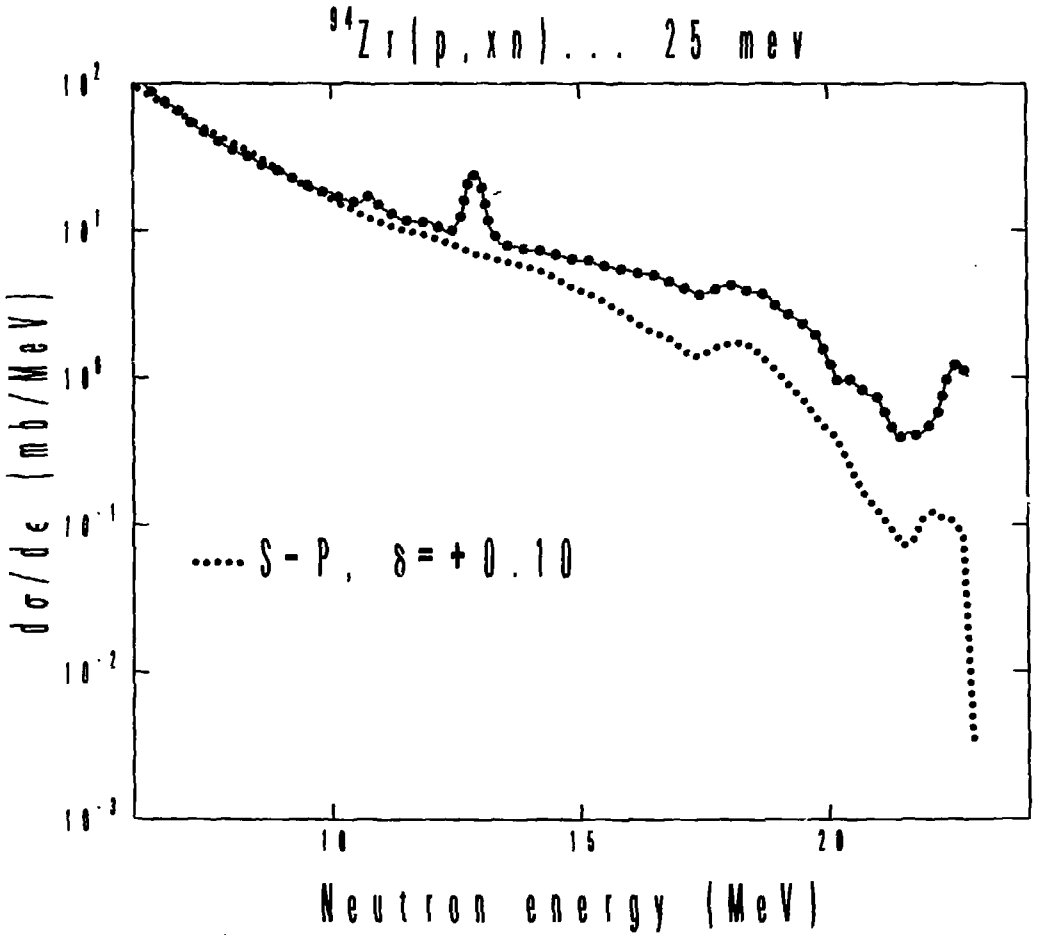
$^{94}Zr(p,xn)\ldots$ 25 mev
10^{2}
10^{1}
10^{0}
10^{-1}
10^{-2}
10^{-3}
$d\sigma/d\epsilon$ (mb/MeV)
..... S - P, $\delta = +0.10$
10
15
20
Neutron energy (MeV)

Figure 13

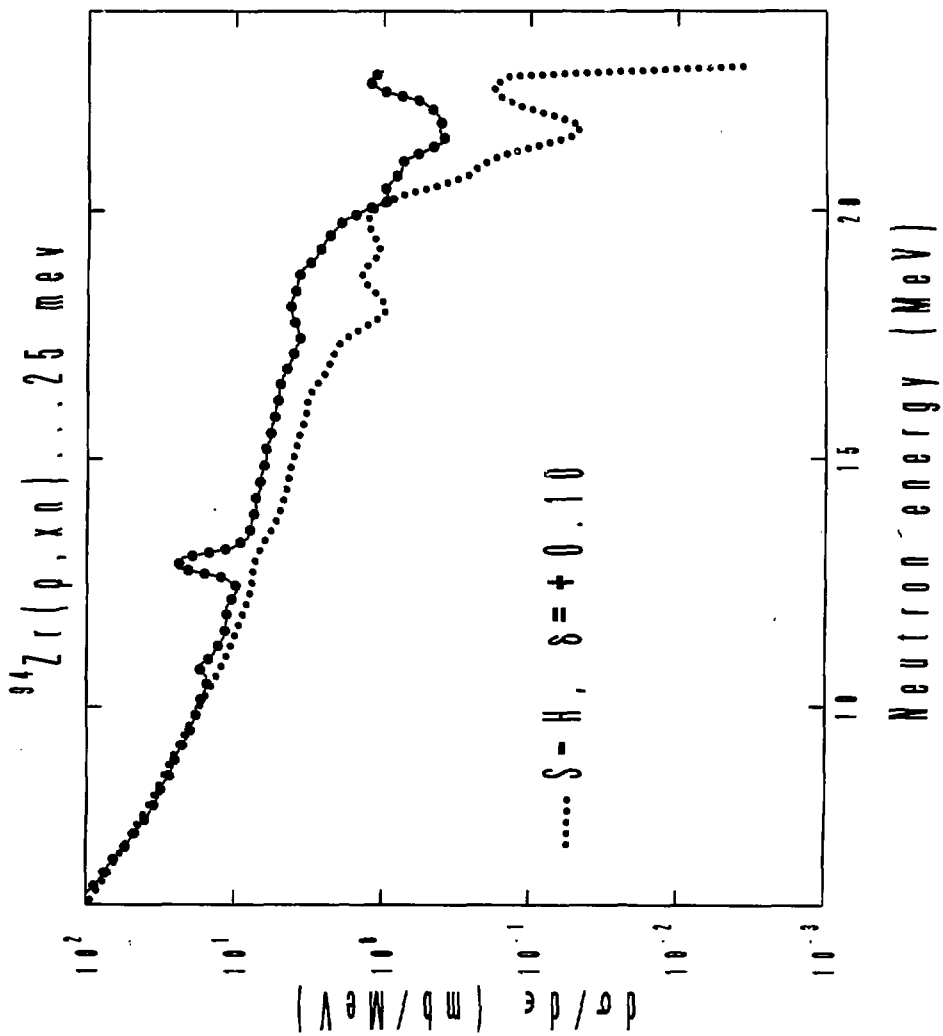
$^{94}Zr(p,xn)$....25 mev
..... S-H, δ=+0.10
$d\sigma/d\varepsilon$ (mb/MeV)
Neutron energy (MeV)
10^{-2}
10^{-1}
10^{0}
10^{-1}
10^{-2}
10^{-3}
10
15
20

Figure 14